catalysts

MDPI

Electronic Supplementary Information

Ultra-Low Loading of Iron Oxide and Platinum on CVD-Graphene Composites as Effective Electrode Catalysts for Solid Acid Fuel Cells

Mhamad Hamza Hatahet,[1] Hagen Bryja ,[2] Andriy Lotnyk,[2] Maximilian Wagner*[2] and Bernd Abel[1]

[1] Wilhelm-Ostwald-Institute for Physical and Theoretical Chemistry, Linnéstr. 3, D-04103 Leipzig, Germany
[2] Leibniz Institute of Surface Engineering, Department Functional Surfaces, 04318 Leipzig, Germany
* Correspondence: Maximilian.wagner@iom-leipzig.de

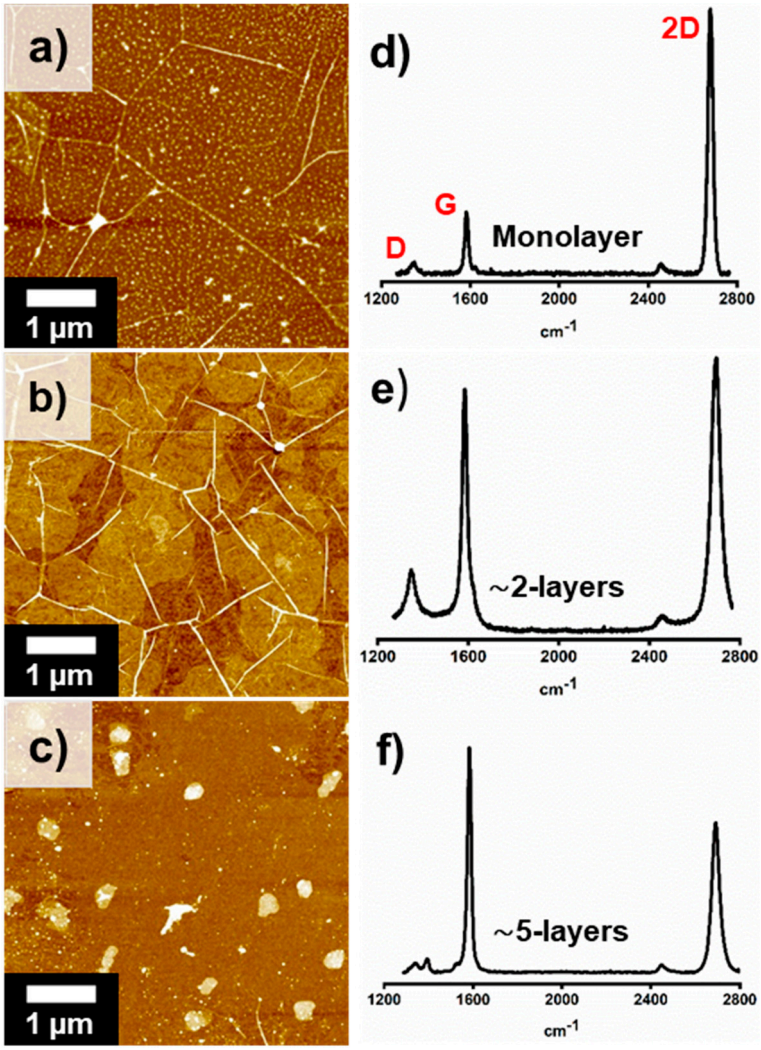

Figure S1. AFM images of as-grown (a) monolayer CVD-graphene, (b) 2L-Gr, (c) 5L-Gr films. Raman spectrum with a 532 nm excitation laser wavelength of (d) monolayer CVD-graphene, (e) 2L-Gr, (f) 5L-Gr films. All CVD-graphene samples transferred on silicon wafer using PMMA and (0.04 M) ammonium persulfate as an etchant. (d) and (f) Reproduced with permission [1].

Higher resolution morphological analyses of the as-grown CVD-graphene on Si-wafer substrate was carried out by tapping mode atomic force microscopy (AFM). Three representative AFM images at three different CVD-graphene layer-thickness (monolayer, ~2-layers and ~5-layers) are shown in Figure S1a, Figure S1b, and Figure S1c respectively. For all samples, submicrometric features can be observed on the CVD-graphene, mainly represented by contaminations (polymer residues, dust) left after removal of the resist film employed for the transfer process. Typical wrinkles can be seen in monolayer and 2L-Gr samples, as indicated in Figure S1a and Figure S1b, respectively. The amount of wrinkles

was significantly reduced by increasing the film thickness to 5L-Gr), as shown in Figure S1c. Corrugations as-grown CVD-graphene film originate from the cooling-down step of the CVD process, due to the different thermal expansion coefficients between CVD-graphene and Cu [2] are also presented mainly at monolayer and 2L-Gr samples. The number of CVD-graphene layers are determined by Raman spectroscopy. The Raman spectrum of different CVD-graphene-thickness samples (Figure S1) reveal three characteristic peaks at ca. 1348, 1590 and 2680 cm^{-1}, which are due to the D, G and 2D (G′) bands, respectively [2]. It is seen that the intensity ratio of G and 2D modes increases with the number of CVD-graphene layers. The increase from 0.23 to 1.48 reveals the increasing of the CVD-graphene layers from monolayer to 5L-Gr [3].

Table S1. Atomic Composition at the surface of the decorated CVD-graphene samples on Si-wafer substrates with different etchants concentrations as determined by XPS with the corresponding Fe mass fraction measured by ICP OES.

Sample	HCl	Q-H_2O	$FeCl_3$	$(NH_4)_2S_2O_8$	Etching Time	Elemental ration (relative atom %)				ICP OES
	(ml)	(ml)	(gr)	(gr)	(h)	Fe	O	C	Si	($\mu gr_{Fe}.cm^{-2}$)
2L-Gr		**100**		**2**	**8**	**0**	**19**	**51**	**30**	**0**
IO(2)@2L-Gr	**10**	**90**	**2**		**8**	**0.2**	**19.4**	**50**	**30.5**	**0.7±0.03**
IO(4)@2L-Gr	**10**	**90**	**4**		**8**	**0.5**	**20.3**	**50.6**	**28.6**	**1.1±0.05**
IO(6)@2L-Gr	**10**	**90**	**6**		**8**	**1.2**	**20.7**	**51**	**27.2**	**2.5±0.2**
IO(8)@2L-Gr	**10**	**90**	**8**		**8**	**1.3**	**20.4**	**51.6**	**26.8**	**2.4±0.3**

The use of hydrochloride solution of iron(III) chloride ($FeCl_3$) for etching the copper foil during the CVD-graphene transfer-process leaves a large amount of iron ions on the CVD-graphene surface [4–6]. The $FeCl_3$ concentration was adjusted in order to control the functionalization density of the CVD-graphene film with iron ions (Table S1). For all experiments, 8 h etching step was applied to dissolve the copper foil completely and decorate the CVD-graphene with varying iron ions loading. Samples nomenclature hereafter follow the system IO(Y)@XL-Gr, where IO is iron oxide (Fe_2O_3), Y is the weight of the iron (III) chloride that was used in the etching solution in gram, X is the number of CVD-graphene layer (L), and Gr is CVD-graphene.

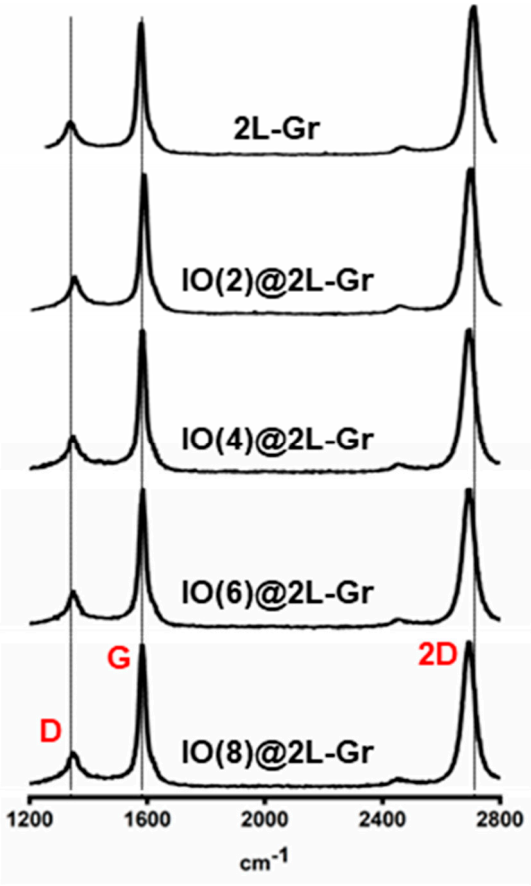

Figure S2. Raman spectra of pristine 2L-Gr and Fe_2O_3 decorated 2L-Gr samples with different concentrations as described in Table S1.

As previously demonstrated in our research group, CVD-graphene surface functionalization and defect formation via O_2 plasma treatment resulted in a significant decrease in electrode impedance [7,8]. As a result, the catalytic activity of the IO(Y)@2L-Gr electrodes has become a contentious issue because it is difficult to determine whether the electrocatalyst activity is due to iron ions or oxygen/defect sites that might be added during the transferring process on the CVD-graphene surface. We defined the catalytic sites on the CVD-graphene surface by analyzing impedance, Raman, and XPS data over the 2L-Gr and IO(Y)@2L-Gr with varying loads of iron ions. Free-iron CVD-graphene, in the presence of surface oxygen-containing groups, shows the lowest hydrogen oxidation activity, with area-normalized electrode resistance (ANR) values of approximately 5800 and 8000 $\Omega.cm^{-2}$ measured after 1 h and 24 h, respectively, as shown in

Figure 3b. The decreasing radius of the semi-circles illustrated in Figure 3 from electrode (b) to electrode (f) indicates lower resistance in electron mobility between the electrode surface [9], when the decoration of iron oxide on CVD-graphene is raised. The electrode activity increases with no significant change in oxygen concentration along the IO(Y)@2L-Gr surfaces (Table S1), indicating that oxygen functional groups do not play a significant role in improving electrochemical efficiency of the system. Aside from the oxygen function groups, Lu et al. [7] reported that defect sites on CVD-graphene samples increase the electrode activity. In Raman spectra of CVD-graphene, G-band and 2D-band represent the carbon sp^2 bonding. In defected CVD-graphene sample and at the edges (cracks), disorder-induced D-band can be measured. The defect concentration was determined from intensity ratio of the Raman D and G peaks [2]. The Raman spectra of 2L-Gr and IO(Y)@2L-Gr membranes are shown in Figure S2. As compared to pristine CVD-graphene, there were no major variations in peak intensity ratios or positions after iron oxide decoration. Figure 3 shows that increasing the Fe_2O_3 loading along the CVD-graphene surfaces causes a decrease in ANR values while leaving the intensities of the three Raman peaks unchanged (Figure S2). These results support the independence of electrode efficiency improvement from CVD-graphene lattice disorders or defects. Because there were no significant changes in oxygen/defect sites on the CVD-graphene surface as a result of the deposition of Fe_2O_3 NPs, it is concluded that iron ions can significantly improve the electrode efficiency of the 2L-Gr during SAFC operation under anodic conditions.

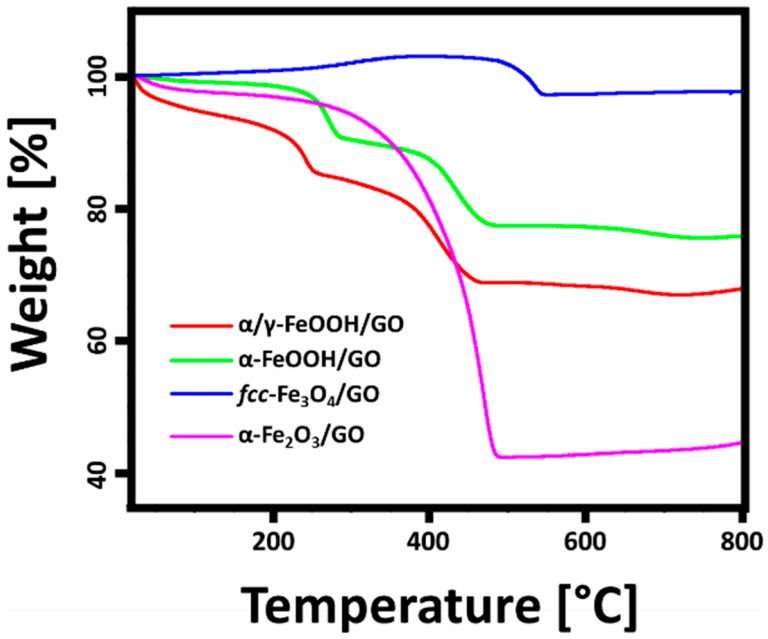

Figure S3. TGA curves of α-Fe_2O_3, Fe_3O_4, α-FeOOH, and α/γ-FeOOH decorated graphene oxide (GO). TGA was performed under air atmosphere. Reproduced with permission [10]. GO is Graphene Oxide.

The weight ratio of iron species in the four composites was investigated using TGA measurements (Figure S3). The weight loss step seen below 120 °C on α/γ-FeOOH/GO, α-FeOOH/GO, and α-Fe_2O_3/GO relates to physical adsorbed water removal [10]. The step of mass loss between 200 and 260 °C for α/γ-FeOOH/GO and α-FeOOH/GO could be assigned to the chemical transformation of FeOOH to Fe_2O_3 in air [10]. It is interesting to find the weight increase of Fe_3O_4/GO composite from 200–400 °C, very likely due to the transformation of Fe_3O_4 to Fe_2O_3. The weight loss observed between 400 and 550 °C for all four samples could be attributed to GO burning [10].

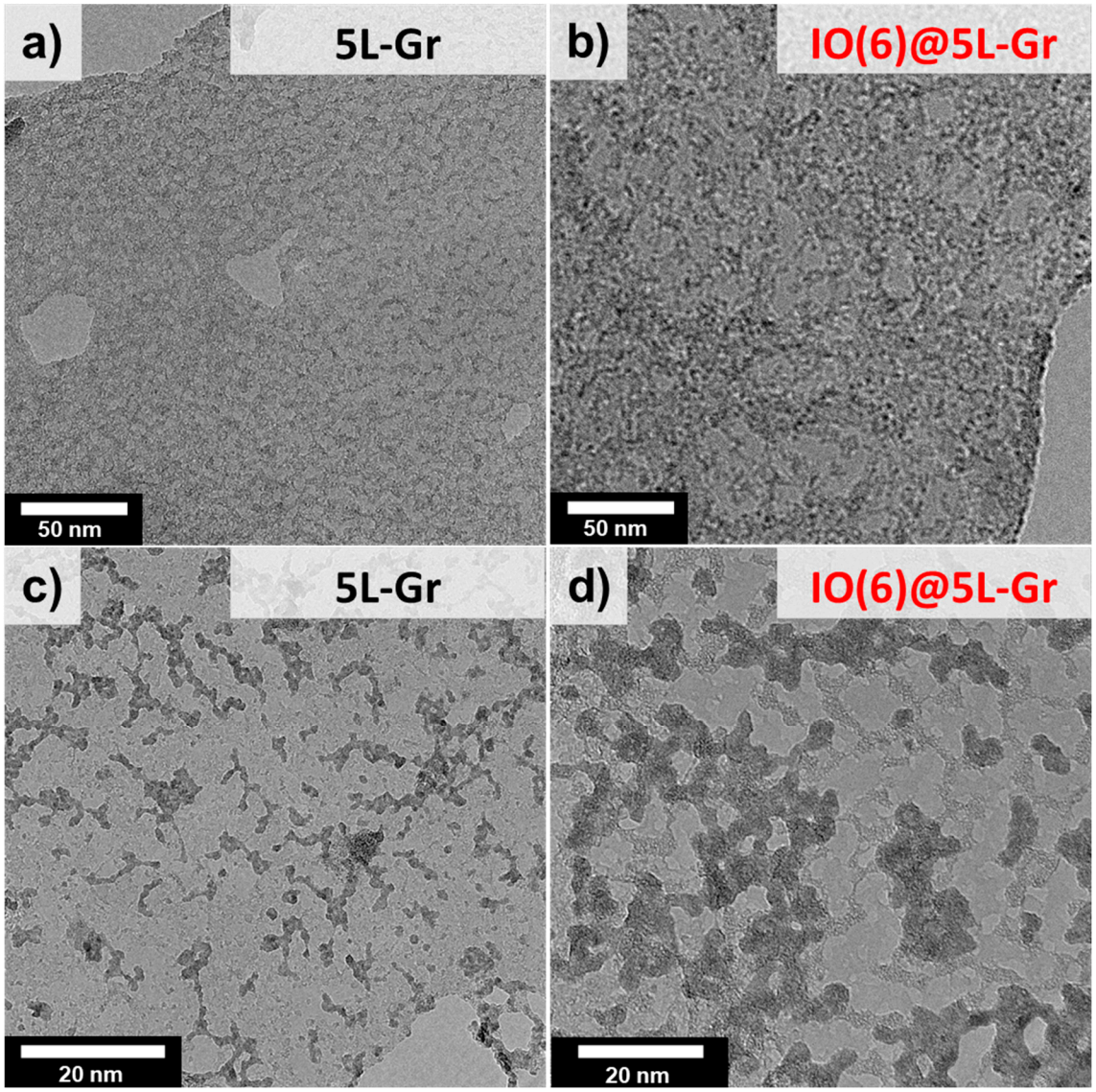

Figure S4. TEM micrographs of 5L-Gr sample transferred using ammonium persulfate as an etchant, low magnification (a), high magnification (c). TEM micrographs of IO(6)@5L-Gr sample, low magnification (b), high magnification (d).

The quality and crystallinity of the bare-graphene and Fe_2O_3 decorated CVD-graphene membranes was investigated by high-resolution TEM, as shown in Figure S4. The wet transfer of CVD-Gr membranes from a growth substrate to a target substrate using poly (methyl methacrylate) (PMMA) is frequently employed in academic circles. Even after removing the polymer with pure acetone and UHV annealing the graphene's sample, Willson *et al*. [11] reported the strong contact between PMMA and the surface of the graphene membranes and demonstrated the existence of PMMA-residues on the graphene surface. To avoid confusion in the TEM image, the graphene samples were transferred onto the grid without

the use of a polymer-based sacrificial layer. The free-polymer transfer enables the analysis of CVD-graphene and iron oxide using TEM and electron beam diffraction without interference from PMMA-residues. It is worth noting that the presence of Fe_2O_3 on the CVD-graphene surface increases the fracture toughness and strength of the CVD-graphene material. We were able to transfer millimeter-size CVD-graphene structures onto the TEM grid, whereas smaller size CVD-graphene sheets (under micrometer) were transferred onto the TEM grid when iron ions were not present.

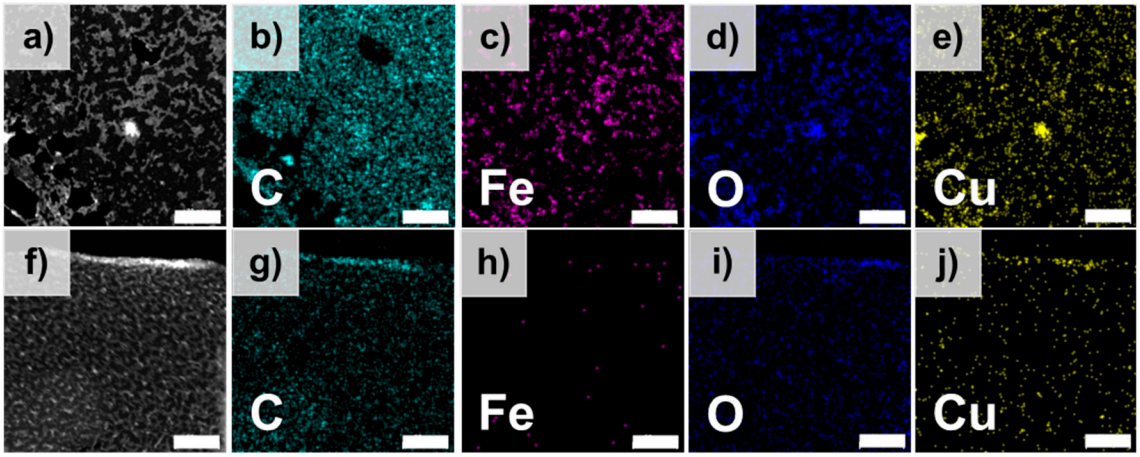

Figure S5. (a) HAADF micrograph of a section of a IO(6)@5L-Gr membrane. (b-e) Elemental mapping images of IO(6)@5L-Gr sample. (f) HAADF micrograph of a section of a 5L-Gr membrane. (g-j) Elemental mapping images of 5L-Gr sample. Scale bar: a-j) 70 nm.

The high-angle annular dark-field imaging (HAADF) and the elemental mapping analysis performed by energy dispersive X-ray (EDX) are shown in Figure S5. The EDX data confirms the presence of carbon, oxygen, iron, chloride and copper on the surface of IO(6)@5L-Gr sample. The atomic percent of C, O, Fe, and Cu are approximately 77, 15.3, 3.2 and 3.3, respectively. The high concentrations of Fe (Figure S5c) and O (Figure S5d), as well as the correlation of their locations, point to the formation of the nano-sized iron oxide islands. According to the map analysis, these as-synthesized iron oxide NPs/islands adsorb and agglomerate on CVD-graphene multiple-islands, whereas no iron oxide NPs can be found on the continuous, pristine, and flat CVD-graphene layers in between, as shown in Figure S4d.

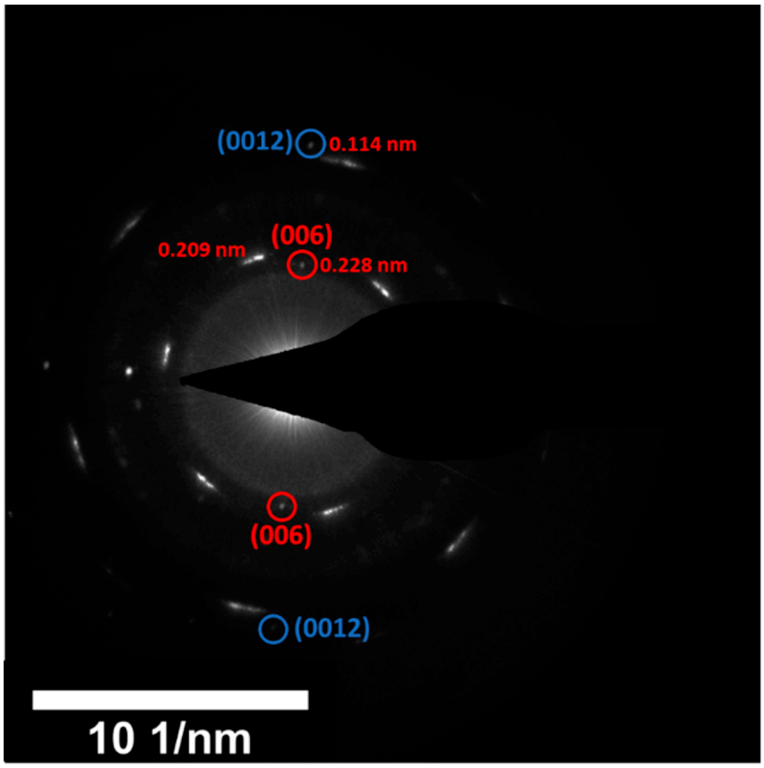

Figure S6. SAED pattern of IO(6)@5L-Gr sample.

Selected area electron diffraction (SAED) was performed to provide detailed information about the iron oxidation state in the IO(6)@5L-Gr sample (Figure S6). The pattern contains diffraction spots attributable to multilayer CVD-graphene. The intensities with the d-spacing of 2.28-2.31 Å are determined and indicate the existence of α-Fe_2O_3 (d(006) = 2.29 Å, ICSD 71194). Additionally, Figure S6 shows an intensity with the d-spacing of 1.14 Å, which agrees well with the d(0012), of the α-Fe_2O_3 (ICSD 71194).

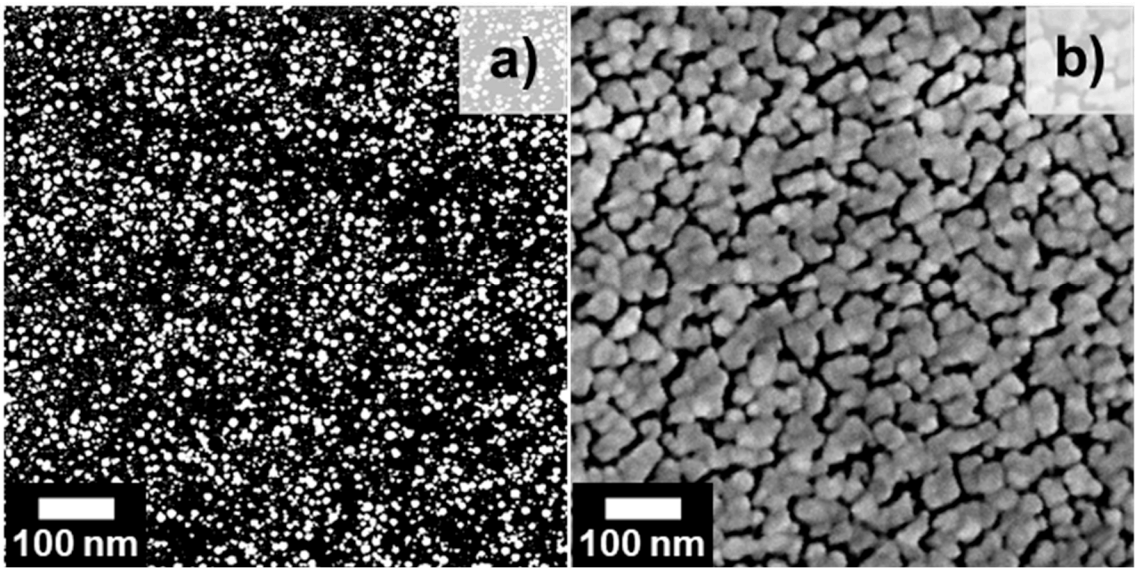

Figure S7. SEM images of 5L-OGr$_{8/100}$ sample after (a) 50 Pt$_{ALD}$ cycles and (b) 200 Pt$_{ALD}$ cycles. All CVD-graphene samples were first oxidized on copper before being deposited with platinum via ALD. Then the Platinum@oxidized CVD-graphene films were transferred on pre-cleaned silicon wafers using PMMA and (0.04 M) ammonium persulfate as an etchant.

The evolution of the Pt$_{ALD}$ NPs on the 5L-OGr$_{8/100}$ surface depending on the number of ALD-cycles [1]. The SEM images after 50 and 200 ALD cycles suggest that the platinum film nucleates on the 5L-OGr$_{8/100}$ substrate as discrete nanoclusters during the early stage of the ALD process, as shown in Figure S7a. As the number of cycles increases, the islands begin to coalesce with adjacent platinum islands to form corrugated and continuous thin-film with worm-like structure at 200 ALD-cycles, as shown in Figure S7b.

References

1. Hatahet, M.H.; Wagner, M.; Prager, A.; Helmstedt, U.; Abel, B. Functionalized and Platinum-Decorated Multi-Layer Oxidized Graphene as a Proton, and Electron Conducting Separator in Solid Acid Fuel Cells. *Catalysts* **2021**, *11*, 947, doi:10.3390/catal11080947.
2. Fisichella, G.; Di Franco, S.; Fiorenza, P.; Lo Nigro, R.; Roccaforte, F.; Tudisco, C.; Condorelli, G.G.; Piluso, N.; Spartà, N.; Lo Verso, S.; et al. Micro- and Nanoscale Electrical Characterization of Large-Area Graphene Transferred to Functional Substrates. *Beilstein J. Nanotechnol.* **2013**, *4*, 234–242, doi:10.3762/bjnano.4.24.
3. Li, P.; Jing, G.; Zhang, B.; Sando, S.; Cui, T. Single-Crystalline Monolayer and Multilayer Graphene Nano Switches. *Appl. Phys. Lett.* **2014**, *104*, 113110, doi:10.1063/1.4868869.
4. Alemán, B.; Regan, W.; Aloni, S.; Altoe, V.; Alem, N.; Girit, C.; Geng, B.; Maserati, L.; Crommie, M.; Wang, F.; et al. Transfer-Free Batch Fabrication of Large-Area Suspended Graphene Membranes. *ACS Nano* **2010**, *4*, 4762–4768, doi:10.1021/nn100459u.
5. Krauß, P.; Engstler, J.; Schneider, J.J. A Systematic Study of the Controlled Generation of Crystalline Iron Oxide Nanoparticles on Graphene Using a Chemical Etching Process. *Beilstein J. Nanotechnol.* **2017**, *8*, 2017–2025, doi:10.3762/bjnano.8.202.
6. Meyer, J.C.; Girit, C.O.; Crommie, M.F.; Zettl, A. Imaging and Dynamics of Light Atoms and Molecules on Graphene. *Nature* **2008**, *454*, 319–322, doi:10.1038/nature07094.
7. Lu, X.; Yang, X.; Tariq, M.; Li, F.; Steimecke, M.; Li, J.; Varga, A.; Bron, M.; Abel, B. Plasma-Etched Functionalized Graphene as a Metal-Free Electrode Catalyst in Solid Acid Fuel Cells. *J. Mater. Chem. A* **2020**, *8*, 2445–2452, doi:10.1039/C9TA10821A.
8. Naumov, O.; Naumov, S.; Abel, B.; Varga, A. The Stability Limits of Highly Active Nitrogen Doped Carbon ORR Nano-Catalysts: A Mechanistic Study of Degradation Reactions. *Nanoscale* **2018**, *10*, 6724–6733, doi:10.1039/C7NR08545A.
9. Yusoff, F.; Suresh, K.; Noorashikin, M.S. Synthesis and Characterization of Reduced Graphene Oxide-Iron Oxide Nanocomposite as a Potential Fuel Cell Electrocatalyst. *IOP Conf. Ser. Earth Environ. Sci.* **2020**, *463*, 012078, doi:10.1088/1755-1315/463/1/012078.
10. Liu, X.; Hu, W. Iron Oxide/Oxyhydroxide Decorated Graphene Oxides for Oxygen Reduction Reaction Catalysis: A Comparison Study. *RSC Adv.* **2016**, *6*, 29848–29854, doi:10.1039/C5RA28038A.
11. Wang, X.; Dolocan, A.; Chou, H.; Tao, L.; Dick, A.; Akinwande, D.; Willson, C.G. Direct Observation of Poly(Methyl Methacrylate) Removal from a Graphene Surface. *Chem. Mater.* **2017**, *29*, 2033–2039, doi:10.1021/acs.chemmater.6b03875.